has been reported for various orthopaedic procedures, such as pelvic osteotomy (10), fixation for acetabular fracture (11), spinal instrumentation (10,12), knee arthroplasty (13) and corrective osteotomy of the upper extremity (14,15), as well as for dental implants (16,17). The surgical guide has a base part to fit on the surgical bone intraoperatively, and a guide part to achieve optimal alignment or position of the surgical instruments on the basis of preoperative computed tomography (CT) images of the relevant bone. Although there is some concern about taking CT images in this technique, some recent papers have reported an improvement to reduce the radiation dose (18,19).

Since the use of the surgical guide for cup insertion has not been reported previously, we applied the surgical guide to dry cadaveric pelvic bones (20). The surgical guide was designed to fit onto intact acetabular edges with the insertion of a Kirschner wire (K-wire) indicating a favourable cup direction. We showed in *the vitro* study that the mean error for the placement of the surgical guide was within 1° [abduction; 0.8° (range 0.2–2.3°, SD 0.8°); anteversion, 0.5° (range 0–2.0°, SD 0.6°)].

The purpose of the current study was to investigate whether the tailor-made surgical guide for cup insertion was useful in real clinical cases.

Materials and Methods

We examined the usefulness of the surgical guide for cup insertion in terms of accuracy of cup insertion and the time required for use of the surgical guide during the operation. The surgical guide for cup alignment was designed preoperatively on the computer using CT images of the patient's pelvis, and then the surgical guide was manufactured using the RP technique. The surgical guide was used during cup insertion in 24 patients. Patient mean age was 65.8 (range 52–87) years; there were two males and 22 females. The preoperative diagnosis was osteoarthritis in 17 patients, osteonecrosis of the femoral head in four patients and rheumatoid arthritis in three patients. This study was approved by the institutional review board, and all patients gave their written informed consent.

Preoperative CT images of the whole pelvis were obtained with a 2.5 mm slice thickness, slice pitch 3 mm (0.15 : 1) and pixel spacing 0.781 mm (Light Speed Plus, GE Medical Systems, Milwaukee, WI, USA). The images were transferred to computer software (3D template, Japan Medical Materials, Osaka, Japan) for 3D planning of the cup. In the software, we acquired any multi-plannar (coronal, sagittal and axial) views with a changing orthogonal coordinate system and any digitally reconstructed plain radiographs (DRR) on each view. The DRR was a synthetic X-ray (21) on the basis of the CT images (Figure 1). To make the pelvic coordinate system, we referenced the supine position of the patients when taking CT images (6,22). With this reference, we could determine the coronal plane corresponding to the plane of the CT table. Then, we defined a line joining the ischial tuberosities as the horizontal axis, with a DRR of anteroposterior direction on the coronal view (Figure 2a). In order to match between preoperative and postoperative pelvic orientations, we recorded the pelvic tilt with another DRR of lateral direction on the sagittal view (Figure 2b) (22) and the angle between the line joining the anterior superior iliac spines and the horizontal line in the axial view (Figure 2c). Abduction of the cup was planned to be 40° using the radiographic definition (23). Anteversion of the cup was planned with a range of 15–20° using the radiographic definition, because acetabular bony coverage and degree of femoral neck anteversion were considered. These angles were defined as the preoperative cup orientation. The matrix data of the cup orientation were recorded for the following process.

The CT images also were transferred to image processing software (Virtual Place-M; Medical Imaging Laboratory, Tokyo, Japan) to reconstruct a polygonal three-dimensional (3D) pelvic model using the marching cubes method (24). The surgical guide was designed by Visualization Toolkit (VTK) libraries (Kitware Inc., Clifton Park, NY, USA). After transferring the pelvic model, the

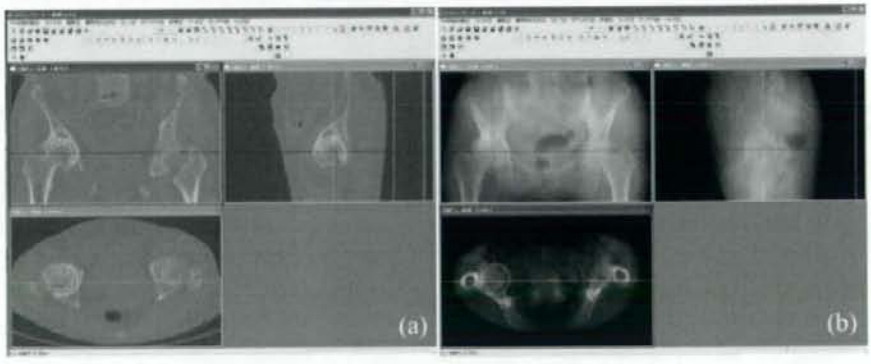

Figure 1. 3D planning of the cup. (a) multi-planar (coronal, sagittal and axial) views of CT images. (b) Digitally reconstructed radiographs on the basis of the CT images. We can acquire these with any orthogonal coordinate system

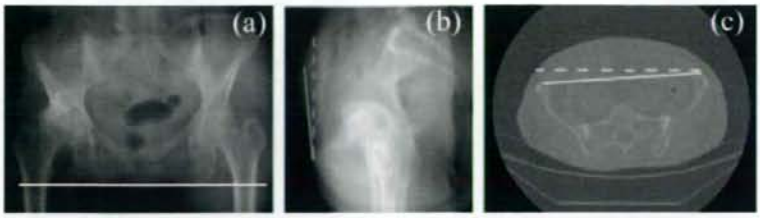

Figure 2. Pelvic coordinate system. (a) The coronal plane corresponded with the plane of the CT table. The line joining the the ischial tuberosities is defined as the horizontal axis (white line). To match between preoperative and postoperative pelvic orientations, the pelvic tilt (b) is the angle between the line of the anatomical plane of the pelvis (solid grey line), through the bilateral superior anterior iliac spines and the superior margin of the pubic symphysis and the vertical line (dotted grey line) on the sagittal view is recorded. The angle (c) between the line (solid white line) joining the bilateral superior iliac spines and the horizontal line (dotted white line) is also recorded

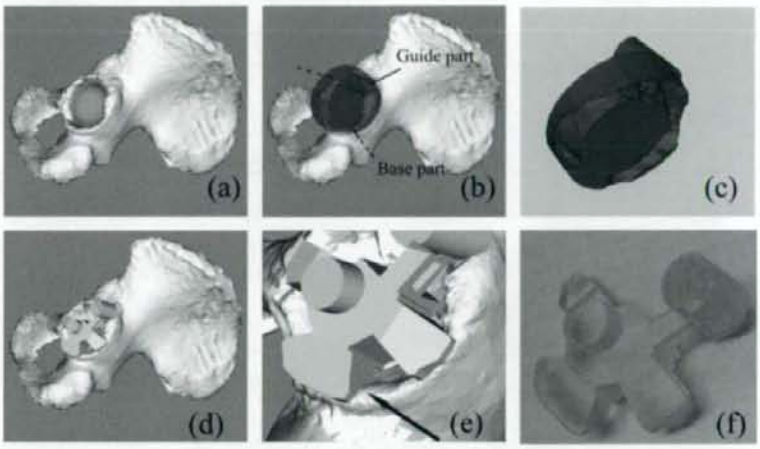

Figure 3. The making of the tailor-made surgical guide. (a) A 3D view of the cup and the pelvic model. (b) Premodel of the surgical guide, which consists of a guide (solid arrow) and base parts (dotted arrow). A broken line shows the alignment of the preoperatively planned cup. (c) Back of the premodel of the surgical guide (when looking from the acetabulum) has an imprint of the acetabular edge after Boolean subtraction. (d) Final model of the surgical guide is made by shaping itself. (e) Some parts used to confirm adaptation between the surgical guide and the acetabular edge are made by shaping of the surgical guide (an arrow indicates one of these confirmation parts). (f) Manufacture of the surgical guide using the RP technique

3D cup model was placed in the acetabulum on the basis of the matrix data (Figure 3a). By the placement of the cup, we could determine some intact parts of the acetabular edge, e.g. inferior parts around the transverse ligament (Figure 3a). The intact parts were used for shaping the surgical guide in the following steps. We designed the premodel of the surgical guide, which consisted of a base and guide parts (Figure 3b: solid arrow, guide part; dotted arrow, base part). The base part, which was a cylindrical object, was placed overlapping the acetabular edge. The guide part was another cylindrical bore and was designed to parallel the direction of the planned cup with its matrix data. The guide part also had cylindrical foramina in order to insert a 2 mm diameter K-wire on the superior acetabulum intraoperatively.

The pelvic model and the premodel of the surgical guide were exported in stereolithography (STL) format to Magics 11 (Materialise NV, Leuven, Belgium) software for spatial image processing to design the surgical guide. The guide part was combined with the base part. The base part was modified by spatially subtracting a part of the acetabular edge from itself, which is known as Boolean subtraction. This modification provided an imprint of the part of the acetabular edge in the base part (Figure 3c). Furthermore, the modified base part was shaped by removing itself partly to fit on only the intact acetabular edges, which were detected by placing the cup on the acetabulum (Figure 3d). Some confirmation points to investigate adaptation between the surgical guide and the acetabular edge intraoperatively were also made consequently by the shaping of the modified base part (Figure 3e; black arrow indicate one of the confirmation parts). The surgical guide was then manufactured with photosensitive medical-grade resin, using an RP machine (Eden 250; Objet Geometries Ltd, Rehovot, Israel; Figure 3f).

The surgical guide was used after femoral head resection, acetabular exposure, and acetabular reaming

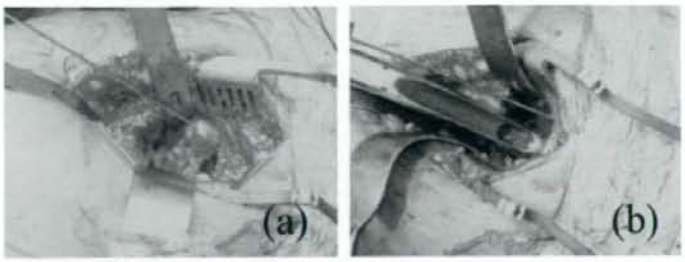

Figure 4. Cinical use of the tailor-made surgical guide during cup insertion of total hip arthroplasty. (a) Placement of the surgical guide and insertion of the K-wire through the guide part. (b) Cup fixation while observing the alignment of the K-wire

during THA. The surgical guide was placed on the periacetabulum (Figure 4a), and the K-wire was inserted on the superior acetabulum through one foramen of the guide part. After removing the surgical guide, cup fixation was performed while observing the alignment of the K-wire (Figure 4b). Since the cup is placed to the hemispherically reamed acetabulum, it was considered that the reaming process hardly affects the alignment errors of the surgical guide. The time from set-up to removal of the surgical guide was recorded. After cup fixation, the remaining steps of the THA, including femoral rasping and stem fixation, were performed using conventional procedures. The operative time and intraoperative blood loss were also recorded.

All patients had a CT scan 3 weeks after surgery. The pelvic coordinate system of the postoperative CT images was determined by the method described above (Figure 2a). The adjustment of the preoperative and postoperative pelvic orientations was performed using information of the preoperative pelvic tilt (Figure 2b) and the angle between the line joining the anterior superior iliac spines and the horizontal line (Figure 2c). The postoperative orientation of the cup was measured after the adjustment. The reproducibility of the measurement of the postoperative orientation of the cup, including in the adjustment between the preoperative and postoperative pelvic orientations, was investigated using the following two parameters, which were used in a previous report (25). Intra-individual (from two measurements separated by a 3-week interval) and inter-individual (by one surgeon and one technical assistant) reliabilities, using Pearson correlation coefficient, and intra- and inter-individual angle differences (absolute angle difference between two measurements) were evaluated. The intra- and inter-individual reliabilities were 0.91 and 0.92 for abduction and 0.94 and 0.88 for anteversion. The intra- and inter-individual angle differences were 1.6° (SD 1.2°) and 1.1° (SD 0.8°) for abduction, and 1.7° (SD 1.3°) and 1.7° (SD 0.9°) for anteversion. 'Cup accuracy', which was defined as the absolute difference between the preoperative cup orientation and the postoperative cup orientation, was measured in all patients.

Results

The mean postoperative orientations of the cup were 38.6° (range 34.0–43.1°; SD 2.7°) of abduction and 17.4° (range 6.3–27.2°; SD 5.6°) degrees of anteversion. The mean cup accuracy was 2.8° (range 0.4–7.7°; SD 2.1°) for abduction and 3.7° (range 0.1–9.3°; SD 2.7°) for anteversion.

The time from set-up to removal of the surgical guide was an average of 3.5 (range 2–6; SD 1.4) min; the mean total operative time was 106 (range 79–169; SD 23.7) min. The intraoperative blood loss was an average of 655 (range 190–1768; SD 330) ml.

Discussion

In the current study, the usefulness of the surgical guide, made using the rapid prototyping technique, to avoid malalignment of the cup was investigated. Although the surgical guide was used in only 24 patients, we consider that the surgical guide was useful in the clinical setting.

It appears that the cup accuracy using the surgical guide was acceptable. Although the mean accuracy of the placement of the surgical guide was <1° in our previous study using dry pelvic bones (20), we assumed that additional errors would occur in the current study with clinical cases. Of these errors, some intrinsic and extrinsic errors are considered (26). In the intrinsic errors, segmentation error was not significant because a previous study reported that the segmentation error was 0.2–0.5 mm with similar CT protocols (with a slice thickness of 4 mm and a pixel spacing of 0.71 mm) (27). The slice thickness (2.5 mm) of the CT images in the current study might increase the intrinsic errors because the slice thickness in our previous study was 1 mm (20). An error from the manufacture of the surgical guide was not significant because the accuracy of printing was 30 μm with high-speed mode and the overall accuracy was 0.1–0.2 mm, according to the brochure or the website of the company which provides the RP machine in the current study (www.objet.com). As to the extrinsic errors, we could address carefully the remove of soft tissues around the periacetabulum, which might affect

the accuracy of the placement of the surgical guide. An error during insertion of the K-wire and adjusting the cup alignment while observing the alignment of the K-wire was within 2°, according to our previous study (20). In addition, press-fit fixation of the cup affects final cup alignment (28). In this previous study on the undesirable effect of the press-fit procedure on the final alignment of the cup, the author showed that the mean absolute cup alignment deviations during implantation were 3.7° of abduction (range 0–9°; SD 2.8°) and 5.1° of anteversion (range 0–10°; SD 2.3°). Although many errors were considered as above, the cup accuracy was, on average, 2.8° for abduction and 3.7° degrees for anteversion. We believe that this cup accuracy achieved by the surgical guide was favourable compared with the following results of conventional and navigated THAs according to previous papers (2–7,29,30).

The mean absolute deviation from preoperative planned alignment of the cup was 4.1–6.3° (maximum 25°) for abduction and 5.2–13.0° (maximum 38°) for anteversion in conventional THAs, and 3.6–4.2 (maximum 15°) for abduction and 4.2–5.3° (maximum 18°) for anteversion in the navigated THAs (2–5,29). With regard to a range within 10° from the desired alignment of the cup, such as the safe zone, 22–71% of the cases with conventional THAs and 80–100% of the cases with the navigated THAs (2–6,30) achieved within the range. The all cup alignments in our study were within 10° from the preoperative planned alignments. Therefore, we consider that our results are more favourable than conventional THAs and comparable to navigated THAs.

We evaluated whether the surgical guide was useful in terms of operating time and blood loss. Although it has been reported that the additional operation time was 15–46 minutes compared with conventional procedures (8,9), the mean time for use of the surgical guide in the current study was about 3.5 min. We consider that this time was not clinically significant. Because the time for the surgical guide was short, the total operation time (average 106 min) and blood loss (average 655 ml) in our study were comparable to some of the previous studies with the conventional and navigated THAs which we evaluated regarding the accuracy of the cup (4,6,7,29,30). The mean total operation time and mean blood loss were 75–178 min and 399–751 ml, respectively, in previous studies with conventional THAs (4,6,7,29) and 83–177 minutes and 341–827 ml in previous studies with navigated THAs (4,6,7,29,30).

Use of the surgical guide maintained the conventional intraoperative procedure. After acetabular reaming, we just placed the surgical guide and inserted the K-wire through the surgical guide. Then, we performed the cup fixation while observing the alignment of the K-wire as the alignment guide for the planned cup. No additional skin incisions for intraoperative registration steps and monitoring space for a computer are needed.

The surgical guide has also some advantages. First, the surgeon can obtain information about cup alignment without looking away from the surgical field. Since most commercial surgical navigation systems display images on a computer monitor positioned adjacent to the surgical field, surgeons might have physical and/or mental difficulty in adjusting between real and computational spatial information, and there may be potential risk to the surgical field while acquiring navigation information on the monitor. We suggest that the procedures involved in using the surgical guide maintain safety, because the surgeon does not have to look away from the surgical field. Second, this surgical guide can be used in any hospital. One needs to only take CT images of the patient, manufacture the surgical guide and sterilize it before the operation. No additional personnel are needed in the operating theatre (10).

There are some drawbacks to the surgical guide. Radiation exposure from the CT scans is a concern. However, it might be justified by the benefits of the imaging information, such as thickness and coverage of the acetabulum and femoral anteversion for implantation in 3D planning. In addition, attempts have been made to develop low-dose radiation CT scans of the pelvis (19). According to a previous paper, the radiation dose for the pelvis with 1–1.5 mm slice thickness was 1.7 mSv, as opposed to 10 mSv for a traditional pelvic CT scan. By comparison, the radiation doses from plain AP and lateral pelvic radiographs are 0.7 and 0.8 mSv, respectively (19). Both preoperative planning and manufacturing of the surgical guide required 90–120 minutes each. Apart from the time for its manufacture, the time for preoperative planning might shorten if dedicated computer software were made for the surgical guide.

In conclusion, the tailor-made surgical guide using the RT technique is useful for cup insertion during total hip arthroplasty in the clinical setting. The mean absolute deviation from preoperative planned alignment of the cup was 2.8° (range 0.4–7.7°; SD 2.1°) for abduction and 3.7° (range 0.1–9.3°; SD 2.7°) for anteversion. All cup alignments were within 10° of the preoperative planned alignments. The intraoperative time for using the surgical guide was an average of 3.5 (range 2–6; SD 1.4) min. Further study is needed to investigate whether the surgical guide provides more accuracy of cup insertion than conventional procedures, without excessive increase of the total operation time and blood loss.

Acknowledgements

This work was supported by grants from the Japan Hip Research Foundation Inc. and Research Fellowship of the Japan Society for the Promotion of Science for Young Scientists. The authors would like to thank Mr Wataru Yamanashi for supporting the technical aspects for this study, Dr Kunihiro Oka and Mr Ryoji Nakao for set-up at the start of this study, Dr Takashi Nishii, Dr Takashi Sakai and Dr Masaki Takao in Osaka University Graduate School of Medicine, Dr Nobuo Nakamura, Dr Akihiro Kakimoto, Dr Daiki Iwana and Dr Makoto Kitada in Kyowakai Hospital for the preliminary study, Dr Kazuo Yonenobu, Dr Mariko Ohshima and Dr Kensuke Ikuta in Osaka Minami Medical Centre for supporting the operative work and Ms Maki Hananouchi for technical assistance.

References

1. Lewinnek GE, Lewis JL, Tarr R, *et al.* Dislocations after total hip replacement arthroplasties. *J Bone Joint Surg Am* 1978; **60**: 217–220.
2. Boosker BH, Verheyen CC, Horstmann WG, *et al.* Poor accuracy of free hand cup positioning during total hip arthroplasty. *Arch Orthop Trauma Surg* 2007; **127**: 375–379.
3. DiGioia AM, Jaramaz B, Plakseychuk AY, *et al.* Comparison of a mechanical acetabular alignment guide with computer placement of the socket. *J Arthroplasty* 2002; **17**: 359–364.
4. Kalteis T, Handel M, Bathis H, *et al.* Imageless navigation for insertion of the acetabular component in total hip arthroplasty: is it as accurate as Ct-based navigation? *J Bone Joint Surg Br* 2006; **88**(2): 163–167.
5. Parratte S, Argenson JN. Validation and usefulness of a computer-assisted cup-positioning system in total hip arthroplasty. A prospective, randomized, controlled study. *J Bone Joint Surg Am* 2007; **89**(3): 494–499.
6. Sugano N, Nishii T, Miki H, *et al.* Mid-term results of cementless total hip replacement using a ceramic-on-ceramic bearing with and without computer navigation. *J Bone Joint Surg Br* 2007; **89**(4): 455–460.
7. Murphy SB, Ecker TM, Tannast M. THA performed using conventional and navigated tissue-preserving techniques. *Clin Orthop Relat Res* 2006; **453**: 160–167.
8. Beringer DC, Patel JJ, Bozic KJ. An overview of economic issues in computer-assisted total joint arthroplasty. *Clin Orthop Relat Res* 2007; **463**: 26–30.
9. Widmer KH, Grützner PA. Joint replacement – total hip replacement with CT-based navigation. *Injury* 2004; **35**(suppl 1): SA84–89.
10. Radermacher K, Portheine F, Anton M, *et al.* Computer assisted orthopaedic surgery with image based individual templates. *Clin Orthop Relat Res* 1998; **354**: 28–38.
11. Brown GA, Milner B, Firoozbakhsh K. Application of computer-generated stereolithography and interpositioning template in acetabular fractures: a report of eight cases. *J Orthop Trauma* 2002; **16**(5): 347–352.
12. Birnbaum K, Schkommodau E, Decker N, *et al.* Computer-assisted orthopedic surgery with individual templates and comparison to conventional operation method. *Spine* 2001; **26**(4): 365–370.
13. Hafez MA, Chelule KL, Seedhom BB, *et al.* Computer-assisted total knee arthroplasty using patient-specific templating. *Clin Orthop Relat Res* 2006; **444**: 184–192.
14. Oka K, Moritomo H, Goto A, *et al.* Corrective osteotomy for malunited intra-articular fracture of the distal radius using a custom-made surgical guide based on three-dimensional computer simulation: case report. *J Hand Surg Am* 2008; **33**(6): 835–840.
15. Murase T, Oka K, Moritomo H, *et al.* Three-dimensional corrective osteotomy of malunited fractures of the upper extremity with use of a computer simulation system. *J Bone Joint Surg Am* 2008; **90**: 2375–2389.
16. Lal K, White GS, Morea DN, Wright RF. Use of stereolithographic templates for surgical and prosthodontic implant planning and placement. Part I. The concept. *J Prosthodont* 2006; **15**(1): 51–58.
17. d'Hauthuille C, Taha F, Devauchelle B, *et al.* Comparison of two computer-assisted surgery techniques to guide a mandibular distraction osteogenesis procedure. Technical note. *Int J Oral Maxillofac Surg* 2005; **34**(2): 197–201.
18. Henckel J, Richards R, Lozhkin K, *et al.* Very low-dose computed tomography for planning and outcome measurement in knee replacement. The imperial knee protocol. *J Bone Joint Surg Br* 2006; **88**(11): 1513–1518.
19. Dandachli W, Kannan V, Richards R, *et al.* Analysis of cover of the femoral head in normal and dysplastic hips. New CT-based technique. *J Bone Joint Surg Br* 2008; **90**(11): 1428–1434.
20. Hananouchi T, Nishii T, Yamanashi W, *et al.* Surgical guide for acetabular insertion using rapid prototyping technique – *in vitro* study. *Int J Computer Assisted Radiology and Surgery* 2008; **3**(suppl 1): S243–S244.
21. Hananouchi T, Sugano N, Nakamura N, *et al.* Preoperative templating of femoral components on plain X-rays. Rotational evaluation with synthetic X-rays on ORTHODOC. *Arth Orthop Trauma Surg* 2007; **127**: 381–385.
22. Nishihara S, Sugano N, Nishii T, *et al.* Measurements of pelvic flexion angle using three-dimensional computed tomography. *Clin Orthop Relat Res* 2003; **444**: 184–192.
23. Murray DW. The definition and measurement of acetabular orientation. *J Bone Joint Surg Br* 1993; **75**(2): 228–232.
24. Lorensen WB, Cline HE. Marching Cubes: A high resolution 3D surface construction algorithm. *Comput Graphics (ACM)* 1987; **21**(4): 163–169.
25. Kalteis T, Handel M, Herold T, *et al.* Position of the acetabular cup – accuracy of radiographic calculation compared to CT-based measurement. *Eur J Radiol* 2006; **58**(2): 294–300.
26. Ruppin J, Popovic A, Strauss M, *et al.* Evaluation of the accuracy of three different computer-aided surgery systems in dental implantology: optical tracking vs. stereolithographic splint systems. *Clin Oral Implants Res* 2008; **19**(7): 709–716.
27. Färber M, Ehrhardt J, Handels H. Automatic atlas-based contour extraction of anatomical structures in medical images. *Int Congr Ser* 2005; **1281**: 272–277.
28. DiGioia AM, Jaramaz B, Blackwell M, *et al.* The Otto Aufranc award. Image guided navigation system to measure intraoperatively acetabular implant alignment. *Clin Orthop Relat Res* 1998; **355**: 8–22.
29. Najarian BC, Kilgore JE, Markel DC. Evaluation of component positioning in primary total hip arthroplasty using an imageless navigation device compared with traditional methods. *J Arthroplasty* 2009; (in press).
30. Hananouchi T, Takao M, Nishii T, *et al.* Comparison of navigation accuracy in THA between the mini-anterior and -posterior approaches. *Int J Med Robotics Comput Assist Surg* 2009; (in press).

SCIENTIFIC ARTICLE

Interosseous Membrane of the Forearm: An Anatomical Study of Ligament Attachment Locations

Kazuo Noda, MD, Akira Goto, MD, PhD, Tsuyoshi Murase, MD, PhD, Kazuomi Sugamoto, MD, PhD, Hideki Yoshikawa, MD, PhD, Hisao Moritomo, MD, PhD

Purpose The interosseous membrane (IOM) of the forearm is a stout ligamentous complex that reportedly comprises several ligamentous components. The purpose of this cadaveric study was to define all IOM ligaments and to clarify the precise attachment locations.

Methods Thirty forearms from 15 embalmed cadavers were used. After dissection, all IOM ligaments were identified, and attachments were measured from the tip of the radial styloid or the ulnar head. Attachment locations were represented as a percentage of total bone length from the distal end of the radius or ulna.

Results The IOM included 5 kinds of ligaments: central band, accessory band, distal oblique bundle, proximal oblique cord, and dorsal oblique accessory cord. The most distal and proximal ends of the radial origin of the central band were 53% and 64% of total radial length from the tip of the radial styloid, whereas those of the ulnar insertion were 29% and 44% of total ulnar length from the ulnar head. The center point of the radial origin and ulnar insertion of the accessory band were 37% and 23%, respectively. The center points of the ulnar origins and radial insertions were 15% and 10% for the distal oblique bundle; 80% and 79% for the proximal oblique cord; and 64% and 62% for the dorsal oblique accessory cord, respectively.

Conclusions The present study clarified precise attachment locations of all representative IOM ligaments. This information will be useful in planning proper graft placement in ligament reconstruction surgery and for future biomechanics research into the function of the IOM ligaments. *(J Hand Surg 2009;34A:415–422. © 2009 Published by Elsevier Inc. on behalf of the American Society for Surgery of the Hand.)*

Key words Anatomy, attachment location, forearm, interosseous membrane (IOM), ligament.

THE INTEROSSEOUS MEMBRANE (IOM) of the forearm is a stout ligamentous complex linking the radius to the ulna. The anatomy of this structure has been studied by various investigators.[1–7] The IOM reportedly consists of distal membranous, middle ligamentous, and proximal membranous portions. Each portion is also known to include several ligamentous components. The most representative component of the IOM is called the central band (CB),[1,2] the broadest and stoutest collection of fibers in the IOM, running obliquely from the proximal radial shaft to the distal ulnar shaft. Prior biomechanical studies[1–3,8–11] have revealed that the CB plays important roles in maintaining forearm functions, as the longitudinal stabilizer of the forearm, and as a load transmitter between the radius and ulna.

The other components of the IOM reportedly comprise the accessory band (AB),[2] which is located adjacent to the CB; the proximal oblique cord[4,5,12–15] on the anterior aspect of the forearm; and the dorsal oblique accessory cord[5] on the posterior side. Some confusion seems to exist with regard to the terminology because prior authors have often used their own terms to repre-

From the Department of Orthopaedic Surgery, Osaka University Graduate School of Medicine, Suita, Osaka, Japan.

Received for publication April 18, 2008; accepted in revised form October 27, 2008.

No benefits in any form have been received or will be received related directly or indirectly to the subject of this article.

Corresponding author: Hisao Moritomo, MD, PhD, Osaka University Graduate School of Medicine, 2-2 Yamadaoka, Suita, Osaka 565-0871, Japan; e-mail: moritomo@ort.med.osaka-u.ac.jp.

0363-5023/09/34A03-0006$36.00/0
doi:10.1016/j.jhsa.2008.10.025

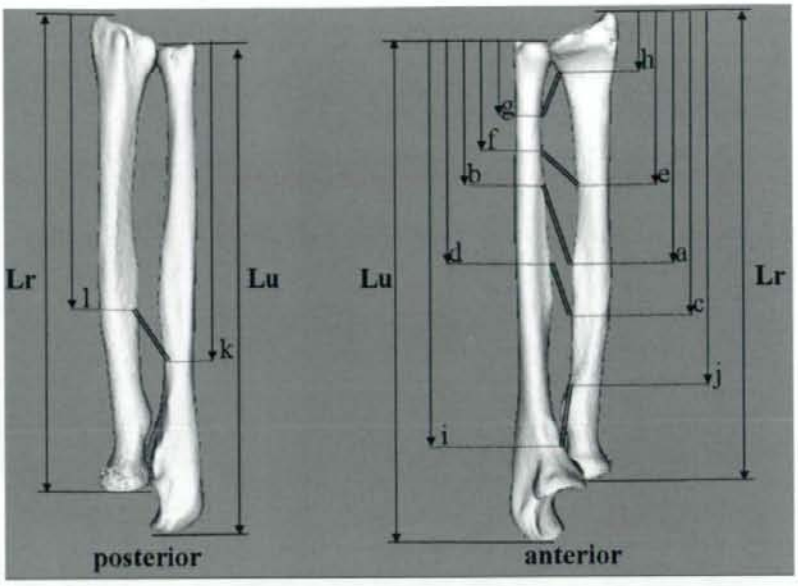

FIGURE 1: Measurement of attachment locations of IOM ligaments. Lr, radial length; Lu, ulnar length. a to l, lengths from the tip of the radial styloid for the radius or from the ulnar head for the ulna. Attachment locations are expressed as percentages of total bone length from the distal end (e.g., a/Lr ×100). a, b and c, d, distal and proximal ends of the central band; e, f, distal ligament of the accessory band; g, h, distal oblique bundle; i, j, proximal oblique cord; k, l, dorsal oblique accessory cord.

sent these structures, and the functions of these ligaments remain a mystery.

IOM researchers have documented the morphological characteristics of the IOM ligaments well, including measurements such as width,[1,2,4,5] thickness,[1,5,6] and insertion angle of the ligament into the radius and ulna.[2,7,16] The purpose of this study was to define all IOM ligaments and to clarify precise attachment locations.

MATERIALS AND METHODS

Thirty forearms from 15 embalmed cadavers (9 females, 6 males) were examined for the width, thickness, and attachment location of the IOM ligaments. Mean age at time of death was 85 years (range, 60–96 years). No apparent pathological lesions were identified in the forearms. The upper extremities were amputated at the middle of the upper arms. Specimens were carefully stripped of all soft tissues remaining on IOM structures and capsuloligamentous tissues around the wrists and elbows. The measurements were made with the forearm positioned in neutral rotation. The width and thickness of each IOM ligament was measured using calipers (accuracy, 0.05 mm; Mitutoyo, Kanagawa, Japan). We then identified the origins (proximal attachments) and insertions (distal attachments) of all ligaments. The locations of the attachments were measured from the tip of the radial styloid for the radius and from the ulnar head for the ulna (Fig. 1). For the CB, both the distal and proximal ends of attachment were measured because it had a broad attachment. For the other ligaments, only the center points of the attachments were measured because they had narrow attachments. A stainless steel ruler (accuracy, 0.15 mm; Shinwa Rules, Niigata, Japan) was used for location measurement. Attachment locations were expressed as percentages of the total bone length of the radius or the ulna from each distal end.

RESULTS

Middle ligamentous complex

The middle portion of the IOM (the middle ligamentous complex) was a complex of ligaments that were quadrilateral in shape and were located within the interosseous space. The middle ligamentous complex was further divided into 2 ligamentous components, the CB and the AB.

Central band: The widest and thickest ligament was the CB, forming part of the middle ligamentous complex (Figs. 2–5). The CB originated from the interosseous

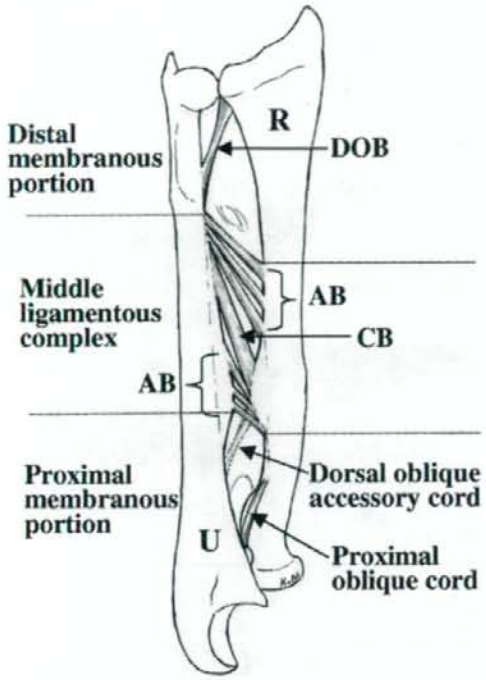

FIGURE 2: Schematic structure of the IOM. Right forearm viewed from the anterior aspect. The IOM consists of distal, middle, and proximal portions. The middle portion is a ligamentous complex (middle ligamentous complex) that is further divisible into the CB and the AB. Distal and proximal portions on either side of the middle portion comprise transparent membranous tissue (distal and proximal membranous portions) with holes for perforation of the interosseous artery. The DOB is present within the distal membranous portion. The proximal oblique cord is present on the anterior side of the forearm and the dorsal oblique accessory cord on the posterior side in the proximal membranous portion. R, radius; U, ulna.

FIGURE 3: Backlit photograph of IOM ligaments. Asterisks indicate the CB as part of the middle ligamentous complex, which originates from the interosseous crest of the radius (white arrow), runs distally and ulnarly, and inserts into the interosseous border of the ulna. Arrows indicate the AB, which runs in a similar way to the CB. Arrowheads indicate the DOB within the distal membranous portion, which originates from around the distal one sixth of the ulnar shaft and inserts into the inferior rim of the sigmoid notch of the radius. Broken arrows indicate the dorsal oblique accessory cord on the posterior aspect of the forearm, which originates from around the distal two thirds of the ulnar shaft and inserts into the interosseous crest of the radius. The proximal oblique cord cannot be distinguished in this photograph because this cord is in contact with the surface of the radial tuberosity (x). R, radius; U, ulna.

crest of the radius, which is the interosseous ridge of the radius that projects most ulnaward, then coursed distally and ulnarly and inserted into the interosseous border of the ulna. The CB was seen in all specimens. The mean width was 9.7 ± 3 mm (range, 4.4–16 mm) measured perpendicular to its fibers, and the mean thickness was 1.3 ± 0.2 mm (range, 1–1.6 mm). The locations of the attachments of the CB on the radius and ulna are detailed in Table 1.

Accessory band: Several ligaments, which were in the same coronal plane as the CB, existed on either side of the CB in the middle ligamentous complex and were collectively termed the AB (see Figs. 2, 3). The fibers of the AB ran in almost the same direction as the CB

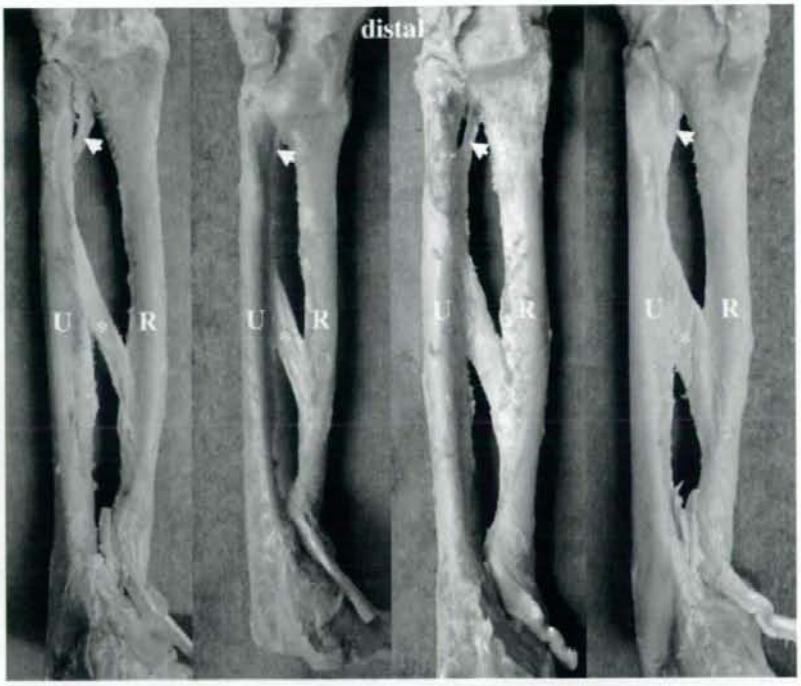

FIGURE 4: The CB and DOB. Four different right forearms are shown. Asterisks indicate the CB, and arrows indicate the DOB. The other ligamentous components were dissected. The CB is the thickest ligament and has a broad attachment. It originates from the interosseous crest of the radius, then courses distally and ulnarly and inserts into the interosseous border of the ulna. The CB was seen in all specimens.

fibers. The structure was less substantial (< 1 mm in thickness) and varied in location and number (Fig. 5). The AB was usually located distal to the CB, and the most distal ligament of the AB tended to be the stoutest of the AB fibers. In comparison, fibers were often absent proximal to the CB, and even if present, they were short and delicate. Of 30 specimens examined, the region distal to the CB showed a single ligament in 14 specimens, 2 ligaments in 3 specimens, 3 ligaments in 8 specimens, 4 ligaments in 1 specimen, 5 ligaments in 1 specimen, and 0 ligaments in 3 specimens. Conversely, the region proximal to the CB showed 0 ligaments in 17 specimens, 2 ligaments in 7 specimens, 3 ligaments in 5 specimens, and 4 ligaments in 1 specimen.

We chose the distal ligament for attachment measurement because it was the only structure of all AB fibers that existed in a relatively constant and stout fashion. The attachment locations of the AB fibers are detailed in Table 1.

Distal membranous portion

The distal membranous portion was on the distal side of the middle ligamentous complex, spanning between the radius and ulna under the region of the pronator quadratus muscle. A hole existed in that portion, through which the interosseous artery passed.

Distal oblique bundle: A relatively thick fiber ran within the distal membranous portion along the distal ulnar shaft in all specimens (see Figs. 2, 3). We named this bundle of fibers the distal oblique bundle (DOB). It existed in the same coronal plane as the CB and AB fibers. Although thickness varied widely among specimens, obvious fibers were seen in 12 of 30 specimens. The DOB originated from approximately the distal one-sixth area of the ulnar shaft, approximately coinciding with the proximal border of the pronator quadratus muscle, and ran distally toward the distal radioulnar joint (DRUJ; Fig. 6). The fibers blended into the capsular tissue of the DRUJ and eventually the DOB inserted to the inferior rim of the sigmoid notch of the

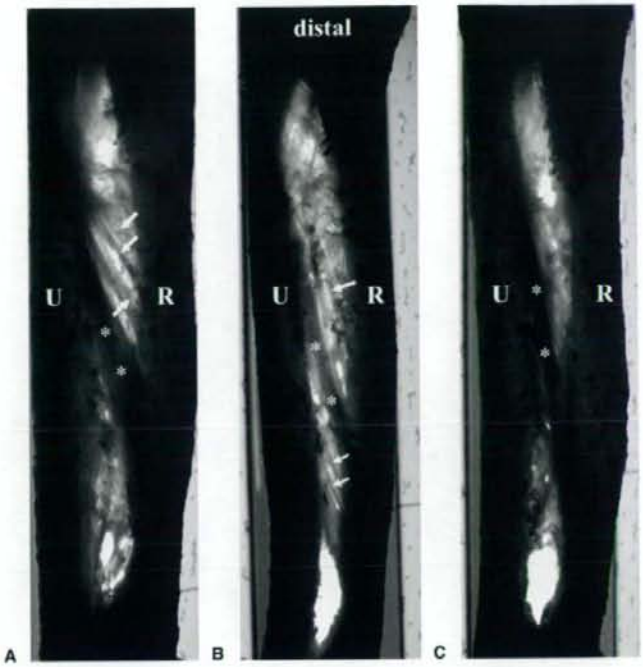

FIGURE 5: The AB. Three different right forearms are shown. Asterisks indicate the CB, and arrows indicate fibers of the AB. The fibers of the AB are less substantial than those of the CB. **A** Pattern of a few AB fibers distal to the CB, without any obvious fibers proximal to the CB. This pattern was seen often. **B** Pattern of AB fibers on either side of the CB. **C** Pattern with no obvious AB fibers on either side of the CB. R, radius; U, ulna.

radius. Furthermore, some fibers extended more distally along the anterior and posterior ridges of the sigmoid notch, so the DOB seemed to display continuity with the dorsal and palmar radioulnar ligaments of the triangular fibrocartilage complex (TFCC). The mean width was 4.4 ± 1.1 mm (range, 2–6 mm) and the mean thickness was 1.5 ± 0.5 mm (range, 0.5–2.6 mm).

The attachment locations of the DOB to the radius and ulna are listed in Table 1.

Proximal membranous portion

The proximal membranous portion was on the proximal side of the middle ligamentous complex. The proximal membranous portion was overlaid by the origin of the flexor digitorum profundus muscle on the anterior aspect of the forearm and by the supinator muscle on the posterior aspect. A hole existed in that portion, through which the interosseous artery passed.

Proximal oblique cord: A ligament called the proximal oblique cord or ligament of Weitbrecht[12,17] was seen in the most proximal interosseous space (Fig. 7; see also Fig. 2) in all specimens. The proximal oblique cord originated from the anterolateral aspect of the coronoid process of the ulna (ulnar tuberosity) and inserted just distal to the radial tuberosity. The proximal oblique cord lay on the surface of the biceps tendon that attaches to the radial tuberosity. The mean width was 3.7 ± 1.6 mm (range, 1.5–8 mm) and the mean thickness was 1.1 ± 0.5 mm (range, 0.4–2 mm).

The sites of attachment of the proximal oblique cord to the radius and ulna are listed in Table 1.

Dorsal oblique accessory cord: A ligament called the dorsal oblique accessory cord was seen on the posterior aspect of the forearm (Fig. 8; see also Figs. 2, 3), located under the origin of the abductor pollicis longus muscle. The dorsal oblique accessory cord was found in 16 of 30 specimens. This ligament originated from around the distal two thirds of the ulnar shaft and inserted into the interosseous crest of the radius. The mean width was 3.2 ± 1 mm (range, 1.9–5 mm), and the mean thickness was 0.9 ± 0.2 mm (range, 0.5–1 mm).

The sites of attachment of the dorsal oblique accessory cord to the radius and ulna are reported in Table 1.

DISCUSSION

Although past researchers have investigated the anatomy of the IOM,[1–7] to say that the history of IOM research is that of the CB is no exaggeration. The CB is frequently discussed in the literature because it is considered the most functional component of the IOM as the result of its stoutness and constancy. The name CB appears to have been first introduced by Hotchkiss and colleagues,[1] but the same formation was also described as the *intermediate descending fiber*[3]; the *cordlike portion*[4,6]; and the *tendinous part*.[5] Many cadaveric studies have been performed to investigate CB function.[1–3,8–11] They have revealed that the CB works as a restraint on the radius from proximal migration in cooperation with the radial head and the TFCC and also works as a load transmitter between the radius and ulna to redistribute load. Other studies[4,17–20] have indicated that the CB is an isometric component of the IOM and shows no change in tension during forearm rotation, thus providing stability to the forearm.

In comparison, the other components of the IOM have been described in only a few studies,[2–5] and their functions remain unclear. Skahen and colleagues[2] reported the AB and the proximal interosseous band, which corresponds to the dorsal oblique accessory cord in the present study. Poitevin[3] reported the proximal ascending bundle, which again corresponds to the dorsal oblique accessory cord in this study.

The functions of the AB have never been described in the literature. However, we suspect from the anatomical variations that function does not extend beyond a complementary nature, probably for the CB.

TABLE 1. Attachment Locations of Interosseous Membrane Ligaments

CB	
Radial origin (distal end)	53 ± 4% (46–61%)
Ulnar insertion (distal end)	29 ± 4% (24–36%)
Radial origin (proximal end)	64 ± 5% (51–74%)
Ulnar insertion (proximal end)	44 ± 5% (34–52%)
Distal ligament of the accessory band	
Radial origin	37 ± 5% (32–46%)
Ulnar insertion	23 ± 3% (19–26%)
DOB	
Ulnar origin	15 ± 2% (13–21%)
Radial insertion	9.9 ± 0.8% (8.3–11%)
Proximal oblique cord	
Ulnar origin	80 ± 2% (76–83%)
Radial insertion	79 ± 2% (75–84%)
Dorsal oblique accessory cord	
Ulnar origin	64 ± 9% (52–83%)
Radial insertion	62 ± 3% (56–68%)

Note: Based on 30 cadaveric forearms. Attachment locations are expressed as percentage of total bone length from the distal end. All data are represented as mean ± SD (range).

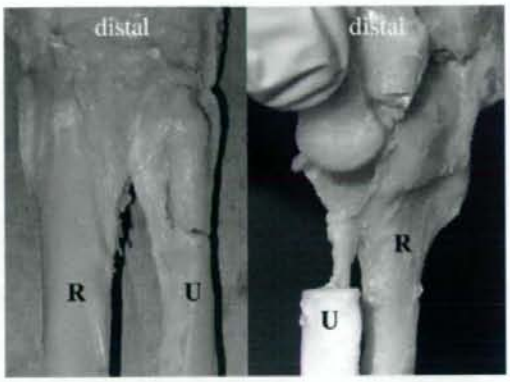

FIGURE 6: The DOB. The photograph on the left shows the DOB as seen from the dorsal aspect of the right forearm. This bundle originates from around the distal one sixth of the ulnar shaft and runs toward the DRUJ. The photograph on the right shows the DOB as seen from the ulnopalmar aspect of the same specimen. The ulna is cut just distal to the ulnar origin of the DOB and retracted distally. The DOB blends into the capsular tissue, through which it inserts into the inferior rim of the sigmoid notch of the radius. R, radius; U, ulna.

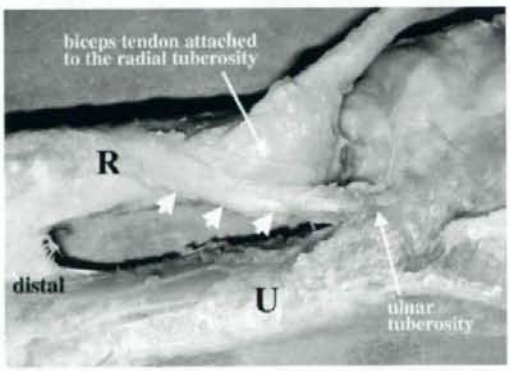

FIGURE 7: The proximal oblique cord. The right proximal forearm as seen from the anteromedial aspect. Arrows indicate the proximal oblique cord, originating from the anterolateral aspect of the coronoid process of the ulna (ulnar tuberosity) and inserting just distal to the radial tuberosity. The proximal oblique cord lies on the surface of the biceps tendon, which is attached to the radial tuberosity. R, radius; U, ulna.

FIGURE 8: The dorsal oblique accessory cord. The right forearm viewed from the dorsal aspect. Arrows indicate the dorsal oblique accessory cord. The dorsal oblique accessory cord exists exclusively on the posterior aspect of the forearm, located under the region of origin of the abductor pollicis longus muscle. The cord originates from around the distal two thirds of the ulnar shaft and inserts into the interosseous crest of the radius (broken line). The dorsal oblique accessory cord was seen in 16 of 30 specimens. R, radius; U, ulna.

We identified the DOB, which was located within the distal membranous portion. Originating from around the distal one sixth of the ulnar shaft and running along the distal ulnar shaft toward the DRUJ, the DOB inserts into the inferior rim of the sigmoid notch of the radius. Furthermore, the DOB seems to exhibit continuity with the dorsal and palmar radioulnar ligaments of the TFCC. Watanabe and colleagues[21] insisted, in their biomechanical study, on the importance of the distal membranous portion of the IOM, which constrained volar and dorsal instability of the radius at the DRUJ in all forearm rotation positions. Kihara and colleagues[22] indicated that the distal membranous portion of the IOM acted as a secondary stabilizer of the DRUJ when the dorsal and palmar radioulnar ligaments of the TFCC were cut. Although we cannot know whether these researchers were aware of the structure of the DOB, we postulate from their studies that the anatomical relationship of the DOB to the TFCC suggests that the DOB functions to stabilize the DRUJ in cooperation with the TFCC because the DOB forms a ligament within the distal membranous portion. However, further biomechanical investigation is needed to confirm our hypothesis.

The proximal oblique cord is a relatively well-investigated component,[13–15,23] whereas descriptions of this ligament are variable. Some authors[23] have insisted that the structure is a remnant or accessory head of the flexor pollicis longus muscle (Gantzer's muscle), whereas another author[13] has stated that this cord represents a thickening of the fascia overlying the supinator muscle or perhaps even a degenerate part of the supinator muscle. We have also observed that the proximal oblique cord shows morphological variations to some extent, ranging from thick to relatively membranous. Conflicting descriptions of function have been reported.[13–15] Martin[13] and Tubbs and colleagues[14] described the cord as being most taut in supination and lax in both the neutral position and pronation in human cadavers, suggesting action as a restraint on excessive supination motions. Conversely, Patel[15] reported that the proximal oblique cord became most taut in pronation rather than in supination in the forelimbs of quadrupedal primates, suggesting a possible role in maintaining elbow stability when such primates stand on their pronated forelimbs. All of these authors concluded that the proximal oblique cord has little function in humans.

The present study clarified precise attachment locations of all representative IOM ligaments. This information will be useful in planning proper graft placement in ligament reconstruction surgery and in future biomechanical research into the function of the IOM ligaments.

REFERENCES

1. Hotchkiss RN, An K-N, Sowa DT, Basta S, Weiland AJ. An anatomic and mechanical study of the interosseous membrane of the forearm: pathomechanics of proximal migration of the radius. J Hand Surg 1989;14A:256–261.
2. Skahen JR III, Palmer AK, Werner FW, Fortino MD. The interosseous membrane of the forearm: anatomy and function. J Hand Surg 1997;22A:981–985.
3. Poitevin LA. Anatomy and biomechanics of the interosseous membrane: its importance in the longitudinal stability of the forearm. Hand Clin 2001;17:97–110.
4. Mori K. Experimental study on rotation of the forearm: functional anatomy of the interosseous membrane. J Jpn Orthop Assoc 1985; 59:611–622.
5. Nakamura T, Yabe Y, Horiuchi Y. Functional anatomy of the interosseous membrane of the forearm: dynamic changes during rotation. Hand Surg 1999;4:67–73.
6. Fujita M. An anatomical study on the interosseous membrane of the forearm. J Jpn Orthop Assoc 1995;69:938–950.
7. Schneiderman G, Meldrum RD, Bloebaum RD, Tarr R, Sarmiento A. The interosseous membrane of the forearm: structure and its role in Galeazzi fractures. J Trauma 1993;35:879–885.

8. Skahen JR III, Palmer AK, Werner FW, Fortino MD. Reconstruction of the interosseous membrane of the forearm in cadavers. J Hand Surg 1997A;22:986–994.
9. Rabinowitz RS, Light TR, Havey RM, Gourineni P, Patwardhan AG, Sartori MJ, et al. The role of the interosseous membrane and triangular fibrocartilage complex in forearm stability. J Hand Surg 1994A;19:385–393.
10. Birkbeck DP, Failla JM, Hoshaw J, Fyhrie DP, Schaffler M. The interosseous membrane affects load distribution in the forearm. J Hand Surg 1997;22A:975–980.
11. Pfaeffle HJ, Stabile KJ, Li ZM, Tomaino MM. Reconstruction of the interosseous ligament restores normal forearm compressive load transfer in cadavers. J Hand Surg 2005;30A:319–325.
12. Kapandji A. Biomechanics of pronation and supination of the forearm. Hand Clin 2001;17:111–122.
13. Martin BF. The oblique cord of the forearm. J Anat 1958;92:609–615.
14. Tubbs RS, O'Neil JT Jr, Key CD, Zarzour JG, Fulghum SB, Kim EJ, et al. Clin Anat 2007;20:411–415.
15. Patel BA. Form and function of the oblique cord *(chorda oblique)* in anthropoid primates. Primates 2005;46:47–57.
16. Chandler JW, Stabile KJ, Pfaeffle HJ, Li ZM, Woo SL-Y, Tomaino MM. Anatomic parameters for planning of interosseous ligament reconstruction using computer-assisted techniques. J Hand Surg 2003;28A:111–116.
17. Hollister AM, Gellman H, Waters RL. The relationship of the interosseous membrane to the axis of rotation of the forearm. Clin Orthop Relat Res 1994;298:272–276.
18. Nakamura T, Yabe Y, Horiuchi Y. In vivo MR studies of dynamic changes in the interosseous membrane of the forearm during rotation. J Hand Surg 1999;24B:245–248.
19. Nakamura T, Yabe Y, Horiuchi Y, Yamazaki N. Three-dimensional magnetic imaging of the interosseous membrane of forearm: a new method using fuzzy reasoning. Magn Reson Imaging 1999;17:463–470.
20. Nakamura T, Yabe Y, Horiuchi Y, Seki T, Yamazaki N. Normal kinematics of the interosseous membrane during forearm pronation-supination: a three-dimensional MRI study. Hand Surg 2000; 5:1–10.
21. Watanabe H, Berger RA, Berglund LJ, Zobitz ME, An KN. Contribution of the interosseous membrane to distal radioulnar joint constraint. J Hand Surg 2005;30A:1164–1171.
22. Kihara H, Short WH, Werner FW, Fortino MD, Palmer AK. The stabilizing mechanism of the distal radioulnar joint during pronation and supination. J Hand Surg 1995;20A:930–936.
23. Forster A. Uber den morphologischen Wert der Chorda oblique antebrachii anterior und der Chorda oblique antebrachii posterior. Z Morphol Anthropol 1905;8:62–79.

Interface focus

J. R. Soc. Interface
doi:10.1098/rsif.2008.0425.focus

REVIEW

Interconnected porous hydroxyapatite ceramics for bone tissue engineering

Hideki Yoshikawa*, Noriyuki Tamai, Tsuyoshi Murase and Akira Myoui

Department of Orthopaedic Surgery, Osaka University Graduate School of Medicine, 2-2 Yamadaoka, Suita 565-0871, Japan

Several porous calcium hydroxyapatite (HA) ceramics have been used clinically as bone substitutes, but most of them possessed few interpore connections, resulting in pathological fracture probably due to poor bone formation within the substitute. We recently developed a fully interconnected porous HA (IP-CHA) by adopting the 'foam-gel' technique. IP-CHA had a three-dimensional structure with spherical pores of uniform size (average 150 μm, porosity 75%), which were interconnected by window-like holes (average diameter 40 μm), and also demonstrated adequate compression strength (10–12 MPa). In animal experiments, IP-CHA showed superior osteoconduction, with the majority of pores filled with newly formed bone. The interconnected porous structure facilitates bone tissue engineering by allowing the introduction of mesenchymal cells, osteotropic agents such as bone morphogenetic protein or vasculature into the pores. Clinically, we have applied IP-CHA to treat various bony defects in orthopaedic surgery, and radiographic examinations demonstrated that grafted IP-CHA gained radiopacity more quickly than the synthetic HA in clinical use previously. We review the accumulated data on bone tissue engineering using the novel scaffold and on clinical application in the orthopaedic field.

Keywords: bone; ceramics; hydroxyapatite; tissue engineering; mesenchymal cell

1. INTRODUCTION

When bone grafts are required for bony defects in orthopaedic surgery, autogenous bone grafting has been the gold standard because of its obvious advantages in osteogenic potential, mechanical properties and the lack of adverse immunological response. On the other hand, autogenous bone grafting has some limitations, such as the requirement of additional surgery for harvesting, the availability of sufficient grafts in size and shape and the risk of donor-site morbidity (Banwart *et al.* 1995; Arrington *et al.* 1996), which may include long-lasting pain, fracture, nerve damage and infection. Although allogeneic bone is widely used in the USA, its use is quite limited in Japan, accounting for as low as 3 per cent of procedures (Prolo & Rodrigo 1985), presumably owing to religious difficulties with using tissue from other people or corpses, as well as the lack of a well-organized tissue bank system. In addition, allograft carries the risk of transmission of occult disease, or a host immune response, which can sometimes result in complete resorption of the grafts. Therefore, many kinds of biomaterials have been developed as bone substitutes, such as hydroxyapatite (HA), alumina, zirconia, bioglass, polymers, metal, and organic or inorganic bone substitutes (Sartoris *et al.* 1986; Bucholz *et al.* 1987; Fujibayashi *et al.* 2003; Nishikawa & Ohgushi 2004).

HA ceramics have been used extensively as a substitute in bone grafts (Holmes *et al.* 1987; Bucholz *et al.* 1989), because the crystalline phase of natural bone is similar to HA. Since the 1980s, blocks and granules of porous calcium HA ceramics (CHA) have been used in orthopaedic, dental or craniofacial surgery (Uchida *et al.* 1990; Yoshikawa & Uchida 1999; Matsumine *et al.* 2004). However, there are few reports which indicate that the pores of implanted CHA are totally filled with the newly formed host bone (Nakasa *et al.* 2005), probably owing to the closed structures of the previous CHA with few interpore connections (Ayers *et al.* 1998).

Therefore, the development of porous CHA with interpore connections of adequate diameter as well as adequate strength has long been expected as an ideal bone substitute (Roy *et al.* 2003; Simon *et al.* 2003, 2007, 2008). We recently developed fully interconnected porous CHA (IP-CHA; porosity 75%, average pore size 150 μm and average interconnections 40 μm) by adopting a 'foam-gel' technique, crosslinking polymerization that gelatinizes through the foam-like slurry in a moment (Tamai *et al.* 2002). The interconnected porous structure facilitates bone tissue

*Author for correspondence (yhideki@ort.med.osaka-u.ac.jp).

Received 11 November 2008
Accepted 28 November 2008

RSIF 20080425—9/12/2008—10:40—SHYLAJA—318693—XML – pp. 1–9

Figure 1. Interconnected porous HA ceramics (IP-CHA). (*a*) Macroscopic images of IP-CHA. The materials were manufactured by Covalent Materials Corporation. (*b*) SEM image of the microstructures of IP-CHA. Spherical pores (100–200 μm in diameter) were divided by thin walls and interconnected by interpores (10–80 μm in diameter).

engineering by allowing the introduction of mesenchymal cells, osteotropic agents or vasculature into the pores. In this review, we report a new bone tissue engineering system using IP-CHA, a preliminary clinical result in patients treated with IP-CHA and a new clinical trial using a prefabricated IP-CHA in orthopaedic surgery.

2. CONVENTIONAL HYDROXYAPATITE CERAMICS IN JAPAN

The crystalline phase of natural bone is basically HA, and HA ceramics have been used extensively as a substitute in bone grafts. The ceramics are available as dense or porous types and the shape types are granular or block-like. Different pore sizes, porosities and strengths are available. Here, we describe four types of conventional HA (the first generation) that were used clinically.

— *BONEFIL* (*Mitsubishi Materials Corporation*). The types of ceramics are porous blocks and porous granules, and are most often used in orthopaedics. The sintering temperature is 900°C and the compression strength is 15 MPa/2 to 3 MPa. The pore shape is spongiose and the pore size is 200–300 μm. The degree of porosity is 60–70 per cent.

— *BONETITE* (*Mitsubishi Materials Corporation*). The types of ceramics are porous blocks and dense granules, and are most often used in dental surgery. The sintering temperature is 1200°C. The pore shape is spongiose and the pore size is 200 μm. The degree of porosity is 70 per cent.

— *BONECERAM* (*Sumitomo Osaka Cement Co., Ltd*). Porous block and porous granular types of the ceramics are available as BONECERAM-P. The sintering temperature is 1150°C. The compression strength is 44.1–68.6 MPa and the bending strength is 12.7–19.6 MPa. The pore shape is spherical and the pore size is 50–300 μm. The degree of porosity is 35–48 per cent. Dense block types of the ceramics having a high mechanical strength are available as BONECERAM-K. The sintering temperature is 1150°C. The bending strength is over 58.8 MPa.

— *APACERAM* (*PENTAX Corporation*). The types of ceramics are both dense and porous. The porous ceramic has a degree of porosity of 15–60 per cent. The sintering temperature is 1200°C. The compression and bending strengths vary from 16 to 250 MPa and 8 to 47 MPa, respectively. The higher mechanical properties are associated with a decrease in the degree of porosity. The pore shape is spherical. The pore structure is an interconnected bimodal pore configuration consisting of a combination of 300 μm macropores and 2 μm micropores. The dense HA has a degree of porosity of less than 0.8 per cent. The sintering temperature is 1050°C. The compression and bending strengths are 750 and 210 MPa, respectively. Clinical applications began in 1985, with approximately 5000 clinical uses of APACERAM ceramics (custom-designed porous type plate) in cranioplasty since then. The numbers of clinical cases involving spinal surgery and ENT surgery with ear ossicle substitutes are 70 000 and 20 000, respectively.

All four of these manufactured HA ceramics are without effective interpore connections and essentially non-resorbable.

3. INTERCONNECTED POROUS HYDROXYAPATITE CERAMICS

The conventional method used to manufacture synthetic porous HA ceramics is by sintering a HA slurry mixed with organic polymer beads (Uchida *et al.* 1984). The polymer beads melt and vaporize during the sintering process, eventually leaving pores in the ceramic material. However, the pores resulting from this method are irregular in size and shape and not fully interconnected with one another. Together with Covalent Materials Corporation, MMT Co., Ltd and National Institute for Materials Science, Biomaterials Center, we developed a fully interconnected porous HA ceramic (IP-CHA; porosity 75%, average pore size 150 μm and average interpore connections 40 μm) by adopting the foam-gel technique (figure 1; Tamai *et al.* 2002). This approach involves a crosslinking polymerization step that gelatinizes the foam-like CHA slurry in a rapid manner, thus promoting the formation of an interconnected porous structure. Briefly, the new method is as follows. (i) Slurry preparation: slurry was prepared by mixing HA (60 wt%) with a crosslinking substrate (polyethyleneimine, 40 wt%). (ii) Foaming and gelatinization: the slurry was mixed with a foaming agent (polyoxyethylene lauryl ether, 1 wt%) and stirred until the mixture had a foamy appearance. Pore size was controlled by regulating the stirring time.

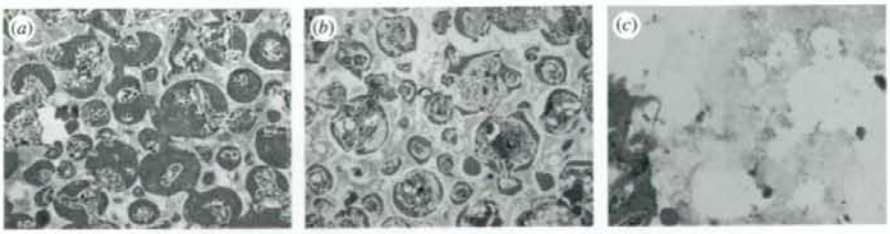

Figure 2. New bone formation within the IP-CHA in the rabbit femoral condyle (HE staining×100). (*a*) Most of the pores were filled with newly formed bone at 2 weeks and (*b*) bone marrow formation was detected at 6 weeks. (*c*) On the other hand, the bone formation was not observed in the control group (conventional HA without interpore connections).

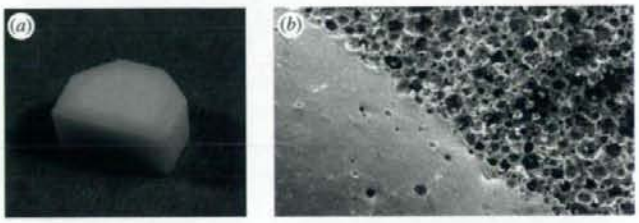

Figure 3. (*a*) Macroscopic and (*b*) microscopic (SEM) images of the solid/interconnected porous HA composite. Mechanical strength of the solid and the porous part is 550–570 and 10–12 MPa, respectively.

(iii) Gelatinization: to gelatinize the foamed slurry, another water-soluble crosslinking agent (polyfunctional epoxy compound) was added and the mixture was cast by pouring into a mould. The porous structure stabilized in less than 30 min. The foamy HA gel was removed from the mould, dried and sintered at 1200°C.

Scanning electron microscopy (SEM) analysis revealed that most of the IP-CHA pores were spherical, similar in size, approximately 100–200 μm in diameter, and showed uniform connections with one another. The wall surface of IP-CHA was very smooth and HA particles were lined closely to one another and bound tightly.

The majority of the interpore connections ranged from 10 to 80 μm in diameter, with a maximum peak of approximately 40 μm, which would theoretically be permissive to cell migration or tissue invasion from pore to pore (Steinkamp *et al.* 1976). Interpore connections larger than 10 μm accounted for as much as 91 per cent of the total porosity in IP-CHA. The calculated available porosity, the proportional volume of pores in the material that were connected by interpore connections larger than 10 μm in diameter, was 73.4 per cent (total porosity)×0.91=67.1 per cent. The compression strength is 12 MPa, while the compression strength of the cancellous bone is 1–12 MPa (Martin *et al.* 1993).

4. OSTEOCONDUCTION *IN VIVO*

Macroporosity is known to influence the biological performance of calcium phosphate *in vivo*. Holmes *et al.* (1988) reported that pores of approximately 100 μm in diameter could provide a framework for bone growth into the pore, which then becomes vascularized easily. Most of the pores of IP-CHA are large enough to show such criteria and, more importantly, the pores are fully interconnected and more likely to allow bone ingrowth. The cylindrical blocks (6 mm in diameter) of IP-CHA were implanted into the rabbit femoral condyle, and the bone ingrowth was histologically analysed (Tamai *et al.* 2002; Myoui *et al.* 2004; Yoshikawa & Myoui 2005). Within six weeks after implantation of IP-CHA, mature bone ingrowth was seen in most of the pores throughout the block. In the pores, bone, bone marrow formation through interpore connections with osteoblastic rimming and vessels were all observed (figure 2). We also examined the sequential change in the compression strength of IP-CHA implanted in rabbit femoral condyle. The initial compression strength of IP-CHA was approximately 10–12 MPa. The implanted IP-CHA steadily increased its compression strength with time until nine weeks after implantation, finally reaching a value of approximately 30 MPa (Tamai *et al.* 2002).

Recently, in order to reinforce its initial mechanical strength, we have developed a novel composite with the solid form of HA. Figure 3 shows the macroscopic and microscopic images of the solid/interconnected porous HA composite (Kaito *et al.* 2006). The mechanical strength of the solid part is 550–570 MPa, thus the solid part may correspond to the cortical bone, and the porous part to the cancellous bone. We constructed the implant and used a canine lumbar interbody fusion model to evaluate bone conduction of the implant and its efficacy for bony fusion. Six months after the surgery, the implant exhibited almost the same efficacy for bony fusion as iliac bone grafts. Moreover, pores of the porous part of the implant were completely filled with newly formed bone and bone marrow cells (Kaito *et al.* 2006).

5. CLINICAL APPLICATION IN ORTHOPAEDIC SURGERY

HA is a useful material to fill the bone defect in treating benign bone tumours because of its biocompatibility,

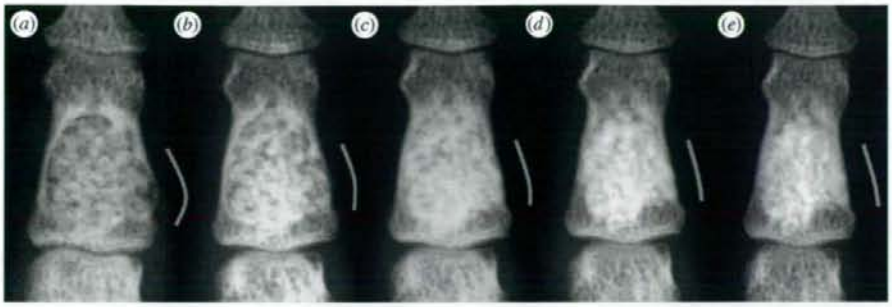

Figure 4. Clinical application of IP-CHA in the treatment of patients with bone tumours. An enchondroma of mid-phalanx, 28-year-old male. As radiodensity increased, the affected bone was remodelled, and the expansive deformity was self-corrected. (*a*) Just after surgery, (*b*) 3 months after surgery, (*c*) 6 months after surgery, (*d*) 12 months after surgery and (*e*) 27 months after surgery.

Figure 5. Clinical application of IP-CHA in the treatment of patients with bone tumours. A simple bone cyst of proximal tibia, 5-year-old boy. (*a*) Before surgery, (*b*) just after surgery, (*c*) 6 months after surgery and (*d*) 36 months after surgery.

osteoconduction and convenience, and it eliminates the additional surgery for harvesting autograft, as we reported previously (Uchida *et al.* 1990; Yoshikawa & Uchida 1999; Matsumine *et al.* 2004). However, as a late complication, pathological fractures of the implanted sites have been reported (Yoshikawa & Uchida 1999; Matsumine *et al.* 2004). This is probably due to poor bone ingrowth in the material as a result of poor incorporation of the material into the host bone. We applied IP-CHA as a bone substitute for the treatment of 59 patients with benign bone tumours at the Osaka University Hospital and its affiliated hospitals. The average age of patients was 32 years (range 5–75 years). The tumours were located in the upper extremities in 25 patients, lower extremities in 27 and pelvis in 7. The mean follow-up period was 46 months (range 32–60 months). After adequate removal of the tumours, IP-CHA blocks and/or granules of 2–5 mm in diameter were used to fill the bony defects. We also used IP-CHA to fill 12 cystic lesions with rheumatoid arthritis (Shi *et al.* 2006). None of the patients showed any signs of inflammatory reaction, rejection, infection or abnormal results in blood tests. Neither pathological fracture nor deformity was observed at the implanted site based on radiographic examinations during the follow-up period. The radiographic examinations were periodically carried out and revealed that the radiolucent line between the implanted IP-CHA and host bone tended to decrease with time after surgery and eventually disappeared (figure 4). The radiographic density at the implanted site increased with time and the IP-CHA granules appeared to fuse with one another, eventually forming a dense radiopaque shadow. Interestingly, longitudinal bone growth was not disturbed even when CHA was implanted in close proximity to the growth plate of children (figure 5). Gadolinium-enhanced MRI showed a ring enhancement at the periphery of the implant (data not shown) and the area with enhancement advanced towards the centre of the implant, indicating that bone regeneration with blood supply might occur within the IP-CHA.

The IP-CHA can be prefabricated into specific sizes and shapes to match bone defects. We performed to make the implant, which was in advance planned and reconstructed with a computer-aided design/manufacturing (CAD/CAM) system. A three-dimensional image was reconstructed with the CT data of the estimated bony defect, and the IP-CHA was fabricated by a three-dimensional milling machine (Roland DG, MDX-20; figure 6). We have used the prefabricated IP-CHA for various bony defects in orthopaedic surgery, and obtained a satisfactory clinical outcome.

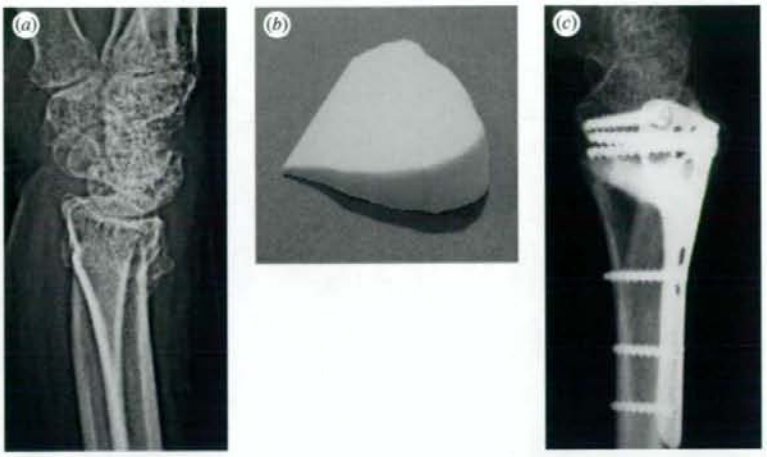

Figure 6. Correction osteotomy for malunited fracture of the distal radius, 48-year-old woman. Preoperative X-ray image of the affected radius, six months after the fracture of the distal radius. (*a*) Prefabricated IP-CHA. A three-dimensional image was reconstructed with the CT data of the estimated bony defect after correction, and the IP-CHA was fabricated by a three-dimensional milling machine (Roland DG, MDX-20). (*b*) Post-operative X-ray image, a year after surgery. The malalignment was satisfactorily corrected by the surgery using the prefabricated IP-CHA and the metal plate.

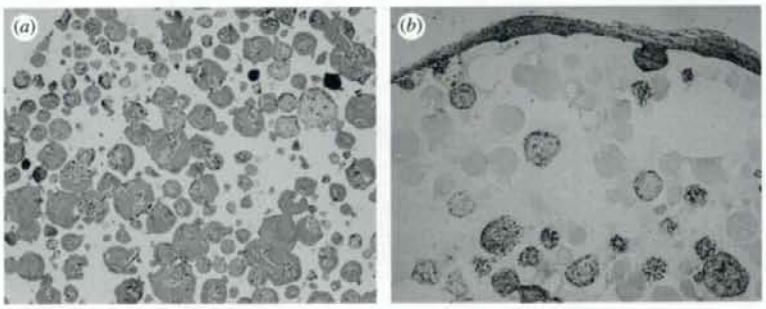

Figure 7. Bone tissue engineering by mesenchymal stem cells (HE staining×40). At eight weeks after implantation, extensive bone volume was detected not only in the surface pore areas but also in the centre pore areas of IP-CHA. (*b*) In the control group (conventional HA without interpore connections), little bone formation was observed even in the surface pore areas.

6. BONE TISSUE ENGINEERING BY MESENCHYMAL STEM CELLS

The IP-CHA can be used as a scaffold for cell-based bone tissue engineering. We tested the efficacy of IP-CHA using a rat subcutaneous model by Ohgushi & Caplan (1999). Bone marrow cells were collected from the femur of rat and were cultivated in minimal essential medium supplemented with 15 per cent foetal bovine serum. IP-CHA discs (R=5 mm, h=2 mm) were soaked in the cell suspension overnight and further cultured in the same medium with β-glycerophosphate, ascorbic acid and dexamethasone for 14 days. The discs were then implanted into the subcutaneous tissue of rats and harvested for two to eight weeks after implantation. All the implants showed bone formation inside the pore areas as evidenced by decalcified histological sections and microcomputed tomography images (Nishikawa *et al.* 2004, 2005). At eight weeks after implantation, extensive bone volume was detected not only in the surface pore areas, but also in the centre pore areas of the implants (figure 7). The combination of IP-CHA and mesenchymal cells could be used as an excellent bone graft substitute because of its mechanical properties and capability of bone formation.

Recently, we have just started a clinical trial with the combination of IP-CHA and autologous mesenchymal cells for bone tissue repair, and already treated 10 patients.

A precise clinical evaluation is necessary, but we believe that bone tissue engineering by IP-CHA offers new approaches to the treatment for patients requiring skeletal reconstruction.

7. BONE TISSUE ENGINEERING BY BONE MORPHOGENETIC PROTEIN

Bone morphogenetic proteins (BMPs) are biologically active molecules capable of inducing new bone formation, and show potential for clinical use in bone defect repair (Wozney & Rosen 1998; Nakase & Yoshikawa 2006).

Figure 8. Bone healing by IP-CHA combined with BMP. (*a*) No implant group at eight weeks after surgery. No bone formation was detected. (*b*) IP-CHA group alone at eight weeks after implantation. Radiolucent lines were clearly visible between IP-CHA and host bone. (*c*) rhBMP-2 (5 μg)/IP-CHA group at eight weeks after implantation. Bony unions were observed at the junction sites and the radiodensity of IP-CHA increased.

However, an ideal system for delivering BMPs that can potentiate their bone-inducing ability and provide initial mechanical strength and scaffold for bone ingrowth has not yet been developed. We have analysed the efficacy of IP-CHA as a delivery system for recombinant human BMP-2 (rhBMP-2). We combined two biomaterials to construct a carrier/scaffold system for rhBMP-2: IP-CHA and a synthetic biodegradable polymer poly-D,L-lactic acid-polyethyleneglycol block co-polymer (PLA-PEG; Miyamoto *et al.* 1993; Saito *et al.* 2001). A rabbit radius model was used to evaluate the bone-regenerating activity of the rhBMP-2/PLA-PEG/IP-CHA composite. All bone defects in groups treated with 5 μg of rhBMP-2 were completely fixed with sufficient strength at eight weeks after implantation (Kaito *et al.* 2005; figure 8). Using this carrier scaffold system, we reduced the amount of rhBMP-2 necessary for such results to approximately one-tenth of the amount needed in previous studies. Enhancement of bone formation is probably due to the superior osteoconduction ability of IP-CHA and the optimal drug delivery system provided by PLA-PEG. The synthetic biodegradable polymer (PLA-PEG)/IP-CHA composite is an excellent carrier/scaffold delivery system for rhBMP-2, and strongly encourages the clinical effects of rhBMP-2 in bone tissue regeneration.

8. BONE TISSUE ENGINEERING BY VASCULAR PREFABRICATION

Vascular network invasion into porous implants is another important aspect of using such materials as bone substitutes for large bone defects or in the construction of tissue-engineered bone, because cells cannot survive farther than a few hundred micrometres from a nutrient supply. The rate of new bone ingrowth into the porous material depends on vascular invasion from the surface of the implant, which is not fast enough in large implants to transport nutrients to cells transplanted in pores of the implant. Therefore, we examined whether prefabrication of IP-CHA with a vascular bundle enhances vascular network invasion into the pores via interpore connections (Akita *et al.* 2004; Myoui *et al.* 2004; Yoshikawa & Myoui 2005). When an IP-CHA cylindrical block was prefabricated with rat superficial inferior epigastric vessels, vascular invasion in the pores increased in both number and size, when compared with the control, resulting in more abundant fibrous connective tissue formation. Our findings suggest that inserting a vascular bundle into such interconnecting porous implants at the site of implantation supports vascular network invasion, which may eventually enhance bone ingrowth in the implants. Nakasa *et al.* (2005) reported that prefabrication of vascularized bone graft using a combination of fibroblast growth factor-2 and vascular bundle implantation into IP-CHA led to a satisfactory result in the reconstruction of the bony defects.

9. APPLICATION FOR CARTILAGE REPAIR AND TENDON ATTACHMENT

We have developed a new technology for articular cartilage repair, consisting of a triple composite of rhBMP-2, PLA-PEG polymer and IP-CHA, to induce the regeneration of both subchondral bone and articular cartilage (Tamai *et al.* 2005). Full-thickness cartilage defects in the rabbit were filled with the rhBMP-2 (20 μg)/PLA-PEG/IP-CHA composite. At six weeks, subchondral defects were completely repaired by subchondral bone and articular cartilage covering the bone. The regenerated cartilage manifested a hyaline-like appearance, with a columnar organization of chondrocytes and a mature matrix. The novel cell-free technology, the triple composite of rhBMP-2, PLA-PEG and IP-CHA could mark a new development in the field of articular cartilage repair. Our new strategy for articular cartilage repair seems to be unique for the following three reasons: (i) we used autogenous mesenchymal cells efficiently recruited

from bone marrow by strongly activating the regeneration process of the subchondral bone defect, (ii) continuous BMP stimuli seemed to promote both the vigorous regeneration of subchondral bone and the following chondrocytic differentiation and cartilaginous matrix production at the surface resulting in hyaline-like cartilage regeneration in as early as three weeks, and (iii) the regenerated cartilage exhibited almost perfect lateral integration with the surrounding host cartilage, probably because the whole regeneration process in this system was *in situ* and efficient, unlike an *ex vivo* chondrocyte culture system. Ito *et al.* (2008) reported that an osteochondral plug using cultured chondrocytes and cylindrical IP-CHA plugs was successful to treat osteochondral defects in a rabbit model. Ohmae *et al.* have also tried to enhance tendon attachment to bone using IP-CHA with bone marrow stromal cells in a rabbit model, and obtained a satisfactory result (Omae *et al.* 2006, 2007).

10. CONCLUSIONS

The foam-gel technique is an innovative method that generates a three-dimensional fully interconnected porous structure in synthetic HA ceramics. The interconnected porous structure encourages bone ingrowth into the material and eventually leads to good incorporation of the material into the host bone. Our study indicated that IP-CHA exhibited excellent bone ingrowth in an animal model and favourable performance in clinical use. We believe that IP-CHA is an excellent bone substitute for filling bone defects and should be considered as an alternative to autogenous bone. In addition, IP-CHA seems likely to serve as a good scaffold for cell-based or cytokine-based tissue-engineered bone. In fact, we have been successful in bone tissue engineering using rhBMP-2, mesenchymal cells or vasculature in animals. The synthetic scaffold can be prefabricated into specific sizes and shapes to match bone defects, and even into a composite with the solid form of HA in order to reinforce its initial mechanical strength. IP-CHA is now commercially available in Japan, and we have applied IP-CHA as a bone substitute for the treatment of more than 80 patients with benign bone tumours or rheumatoid arthritis, and obtained some favourable clinical results. Recently, we have started a clinical trial with the combination of IP-CHA and autologous mesenchymal cells for bone tissue repair. Additional studies with larger animals including dogs or monkey and precise clinical evaluation are necessary, but we believe that bone tissue engineering by IP-CHA offers new approaches to the treatment for patients requiring skeletal reconstruction.

The authors would like to thank Dr Kunio Takaoka for his invaluable advice regarding bone tissue engineering using rhBMP-2, and Dr Hajime Ohgushi for his invaluable advice regarding bone tissue engineering using bone marrow cells. We also thank Covalent Materials Corporation and MMT Co., Ltd for supplying materials. This work was supported in part by grants from New Energy and Industrial Technology Development Organization (NEDO), the Ministry of Health, Labor and Welfare, Japan, and the Ministry of Education, Culture, Sports, Science and Technology, Japan.

REFERENCES

Akita, S., Tamai, N., Myoui, A., Nishikawa, M., Kaito, T., Takaoka, K. & Yoshikawa, H. 2004 Capillary vessel network integration by inserting a vascular pedicle enhances bone formation in tissue-engineered bone using interconnected porous hydroxyapatite ceramics. *Tissue Eng.* **10**, 789–795. (doi:10.1089/1076327041348338)

Arrington, E. D., Smith, W. J., Chambers, H. G., Bucknell, A. L. & Davino, N. A. 1996 Complications of iliac crest bone graft harvesting. *Clin. Orthop.* **329**, 300–309. (doi:10.1097/00003086-199608000-00037)

Ayers, R. A., Simske, S. J., Nunes, C. R. & Wolford, L. M. 1998 Long-term bone ingrowth and residual micro hardness of porous block hydroxyapatite implants in humans. *J. Oral. Maxillofac. Surg.* **56**, 1297–1301. (doi:10.1016/S0278-2391(98)90613-9)

Banwart, J. C., Asher, M. A. & Hassanein, R. S. 1995 Iliac crest bone graft harvest donor site morbidity. A statistical evaluation. *Spine* **20**, 1055–1060. (doi:10.1097/00007632-199505000-00012)

Bucholz, R. W., Carlton, A. & Holmes, R. E. 1987 Hydroxyapatite and tricalcium phosphate bone graft substitute. *Orthop. Clin. North Am.* **18**, 323–334.

Bucholz, R. W., Carlton, A. & Holmes, R. 1989 Interporous hydroxyapatite as a bone graft substitute in tibial plateau fractures. *Clin. Orthop.* **240**, 53–62.

Fujibayashi, S., Kim, H. M., Neo, M., Uchida, M., Kokubo, T. & Nakamura, T. 2003 Repair of segmental long bone defect in rabbit femur using bioactive titanium cylindrical mesh cage. *Biomaterials* **24**, 3445–3451. (doi:10.1016/S0142-9612(03)00221-7)

Holmes, R. E., Bucholz, R. W. & Mooney, V. 1987 Porous hydroxyapatite as a bone graft substitute in diaphyseal defects: a histometric study. *J. Orthop. Res.* **5**, 114–121. (doi:10.1002/jor.1100050114)

Holmes, R. E., Wardrop, R. W. & Wolford, L. M. 1988 Hydroxylapatite as a bone graft substitute in orthognathic surgery: histologic and histometric findings. *J. Oral. Maxillofac. Surg.* **46**, 661–671. (doi:10.1016/0278-2391(88)90109-7)

Ito, Y., Adachi, N., Nakamae, A., Yanada, S. & Ochi, M. 2008 Transplantation of tissue-engineered osteochondral plug using cultured chondrocytes and interconnected porous calcium hydroxyapatite ceramic cylindrical plugs to treat osteochondral defects in a rabbit model. *Artif. Organs* **32**, 36–44.

Kaito, T., Myoui, A., Takaoka, K., Saito, N., Nishikawa, M., Tamai, N., Ohgushi, H. & Yoshikawa, H. 2005 Potentiation of the activity of bone morphogenetic protein-2 in bone regeneration by a PLA-PEG/hydroxyapatite composite. *Biomaterials* **26**, 73–79. (doi:10.1016/j.biomaterials.2004.02.010)

Kaito, T., Mukai, Y., Nishikawa, M., Ando, W., Yoshikawa, H. & Myoui, A. 2006 Dual hydroxyapatite composite with porous and solid parts: experimental study using canine lumbar interbody fusion model. *J. Biomed. Mater. Res. B* **78**, 378–384. (doi:10.1002/jbm.b.30498)

Martin, R. B., Chapman, M. W., Sharkey, N. A., Zissimos, S. L., Bay, B. & Shors, E. C. 1993 Bone ingrowth and mechanical properties of coralline hydroxyapatite 1 yr after implantation. *Biomaterials* **14**, 341–348. (doi:10.1016/0142-9612(93)90052-4)

Matsumine, A., Myoui, A., Kusuzaki, K., Araki, N., Seto, M., Yoshikawa, H. & Uchida, A. 2004 Calcium hydroxyapatite